JGR Atmospheres

RESEARCH ARTICLE
10.1029/2023JD039942

Electrical Alignment Signatures of Ice Particles Before Intracloud Lightning Activity Detected by Dual-Polarized Phased Array Weather Radar

Shuo Wang[1], **Yuuki Wada**[1], **Syugo Hayashi**[2], **Tomoo Ushio**[1], **and V. Chandrasekar**[3]

[1]Osaka University, Suita, Japan, [2]Meteorological Research Institute, Japan Meteorological Agency, Tsukuba, Japan, [3]Colorado State University, Fort Collins, CO, USA

Key Points:

- The electrical alignment signatures strengthen before the first intracloud lightning flash and weaken following with it
- The composite K_{DP} is introduced to analyze the electrical alignment signatures of ice crystals in thunderstorms
- Electrical alignment signatures of ice crystals could be a good indicator of initial electrification

Correspondence to:
S. Wang,
wang@se.eei.eng.osaka-u.ac.jp

Citation:
Wang, S., Wada, Y., Hayashi, S., Ushio, T., & Chandrasekar, V. (2024). Electrical alignment signatures of ice particles before intracloud lightning activity detected by dual-polarized phased array weather radar. *Journal of Geophysical Research: Atmospheres*, *129*, e2023JD039942. https://doi.org/10.1029/2023JD039942

Received 10 OCT 2023
Accepted 19 MAR 2024

Author Contributions:
Conceptualization: Tomoo Ushio, V. Chandrasekar
Funding acquisition: Tomoo Ushio
Investigation: Yuuki Wada, Syugo Hayashi
Resources: Syugo Hayashi
Supervision: Tomoo Ushio
Validation: Yuuki Wada
Writing – review & editing: Yuuki Wada

Abstract The cloud electrification process has great significance in understanding the microphysical properties, electrical characteristics, and evolution of thunderstorms. This study employs an X-band dual-polarized multiparameter phased array weather radar (MP-PAWR) to observe the electrical alignment signatures of ice particles before the first intracloud (IC) lightning flash, and to explore the evolution of the upper charge region in the early electrification stage of an isolated thunderstorm. Negative K_{DP} signatures associated with vertically oriented ice particles by strong electric fields in the upper parts of the thunderstorm are analyzed by introducing composite K_{DP}, which is defined as a minimum K_{DP} value observed in a vertical column across all elevation scans at each specific horizontal grid point at and above a designated layer. About 7 min before the first IC lightning flash, the mean canting angle of ice particles in the upper parts of the cloud changed from horizontal to vertical by strong electric fields, and the concentration of vertically aligned ice particles on the top of the cloud reached the maximum 30 s before the first IC lightning flash. These signatures exhibit an early electrification process in the upper parts of the thunderstorm. These results indicate that with the high spatial and temporal resolution, MP-PAWRs have the ability not only to detect the rapid evolution of microphysical structures but also to observe the early electrification of thunderstorms, which will facilitate forecasting IC lightning flash initiation combined with graupel presence signatures in the mixed-phase region in normal operation.

Plain Language Summary The electrical alignment signatures of ice particles in the upper parts of the thunderstorms refer to the changes in the orientation of ice particles due to the variation of in-cloud electric fields, which offer useful information in understanding the cloud electrification process. Based on the lightning data and observations from an X-band dual-polarized multiparameter phased array weather radar (MP-PAWR) with high temporal and spatial resolution, the signatures related to the electrically aligned ice particles before the first intracloud (IC) lightning flash are analyzed, and the results show that the electrical alignment signatures of ice crystals could be a good indicator of initial electrification related to the upper charge region. These findings hold potential significance in enhancing lightning forecasting capabilities.

1. Introduction

The cloud electrification process plays an important role in understanding microphysical, electrical properties and evolution of thunderstorms and lightning activity. According to the non-inductive charging theory, which is the most viable explanation for the initial electrification of thunderstorms, it is widely accepted that the transfer of electrical charge occurs during collisions between graupel and smaller ice crystals in the presence of supercooled water within the storm's mixed-phase region which typically ranges from about 0°C to −40°C (Takahashi, 1978; Takahashi & Miyawaki, 2002; Williams, 1989). The negatively charged graupel accounts for the main negative charge region distributes at approximately constant temperature levels between −10°C and −20°C, while positively charged ice particles move upward by updraft to form the upper positive charge region (Dye et al., 1986, 1988; Krehbiel, 1986; Saunders, 1993; Saunders et al., 2006; Workman & Reynolds, 1949). Numerous previous studies have explored the relationship between precipitation development and electrical characteristics in thunderstorms by weather radar (Bringi et al., 1997; Buechler & Goodman, 1990; Carey & Rutledge, 2000; Dye et al., 1989; Gremillion & Orville, 1999; Larsen & Stansbury, 1974; Lund et al., 2009; Williams et al., 1989). They utilized the reflectivity at different temperature levels in the mixed-phase region and the kinematic structure of clouds to investigate the initiation of thunderstorms, as well as the onset of

electrification in thunderstorms and forecasting of lightning activity. Typically, in these studies, the formation of the main negative charge region within storms, characterized by the presence of graupel during the updraft, was considered a reliable indicator of initial electrification. In contrast, the features associated with the upper positive charge region which consists of charged ice particles, despite being an integral part of thunderstorm electrification, gained less attention in studying the initial electrification.

As the two primary charge separation theories proposed to explain electrification in the cloud, both the inductive and non-inductive charging mechanisms normally cause ice crystals in a thunderstorm to become positively charged and graupel to become negatively charged (Aufdermaur & Johnson, 1972; Brooks & Saunders, 1994; Reynolds et al., 1957; Saunders, 2008; Takahashi, 1978; Takahashi & Miyawaki, 2002). Due to the size differences, the charged ice crystals are carried aloft to accumulate the upper positive charge region, while the graupel tends to fall or be suspended by the updraft to form the main negative charge region below. The small ice crystals on the top of the cloud, such as plate, column, and needle shapes, could be oriented vertically with their principal axis by the strong electric fields. This sign was first observed as an unusual optical phenomenon in 1950, the vertically aligned ice crystals reflect the light from their horizontal surfaces like small mirrors. Vonnegut (1965) mentioned this phenomenon could have resulted from changes in the alignment of ice crystals due to the strong electric field within thunderstorms. An optical polarization measurement was made by Mendez (1969), and the results showed that "the electric field contained within the thunderstorm prior to and after a lightning discharge is imaged by the local degree of polarization produced by the sunlight reflected from oriented ice crystals on the surface of the storm."

The changes of differential propagation and backscatter characteristics that arise from electrical vertically aligned ice crystals on the top of the cloud provide more polarized information to study the electrification and lightning activities in thunderstorms by weather radar observation. The earliest observations of the polarized parameter signatures related to such electrical alignment of ice particles were mainly performed with circularly polarized weather radars. Abrupt changes in the polarization parameters associated with lightning flashes were first observed in 1974 (Hendry & McCormick, 1976), and Hendry and McCormick (Hendry & McCormick, 1976; McCormick & Hendry, 1979) showed the existence of vertically canted ice particles in the upper parts of thunderstorms before lightning discharges by a Ku-band circular-polarization radar. They concluded that the abrupt changes in orientation and circular depolarization ratio were induced by the lightning discharges. Further research by Hendry (Hendry & Antar, 1982) showed that the depolarization effects in some cases could probably be caused by the propagation effects of radiowaves in the particles which are too small to be detected by radar. Similar observations were obtained by using S-band (Metcalf, 1992, 1993, 1995) and X-band (Krehbiel & Gray, 1993; Krehbiel et al., 1992, 1996) circular polarimetric radar, respectively. These studies showed that the changes in propagation effects were associated with rapid changes in orientations of hydrometeors in the middle and upper parts of the cloud caused by electric fields. The mean canting angle of the hydrometeors is near 90° before lightning and subsequently recovers to the horizontal orientation following a lightning discharge.

The depolarization effects related to the electrical alignment of ice particles have also been observed by dual-linear polarized weather radars (Caylor & Chandrasekar, 1996; Hubbert et al., 2014; i Ventura et al., 2013; Mattos et al., 2016, 2017; Krehbiel et al., 2005; Ryzhkov & Zrnić, 2007; Schvartzman et al., 2022; Scott et al., 2001; Zrnic & Ryzhkov, 1999). By observing with a dual-wavelength (S-band and X-band) dual-linear polarized weather radar, the first measurement of the specific differential phase (K_{DP}) related to the orientation of ice particles with in-cloud electric fields has been taken by Caylor and Chandrasekar (1996). The study implied that K_{DP} and linear depolarization ratio (LDR) can be used to investigate the orientation of ice crystals in the upper parts of thunderstorms by in-cloud electric fields and roughly concluded the relation of LDR and K_{DP} to ice crystal orientation angle. The negative K_{DP} corresponds to the vertically aligned ice particles due to strong electric field, while positive K_{DP} associates with horizontal alignment ice particles. The study showed that no orientation-related signatures were observed in the copolar correlation coefficient (ρ_{HV}) and differential reflectivity (Z_{DR}) of the S-band. It indicates that the polarimetric signatures are caused primarily by propagation effects. The period changes in K_{DP} can be attributed to variations in the alignment of ice crystals, which tend to align parallel to the in-cloud electric fields. K_{DP} decreases gradually on the top of the cloud as the electric field accumulates, then suddenly increases coincident with lightning discharges. Besides the negative K_{DP} signatures associated with vertically aligned ice particles in the in-cloud electric fields, the Z_{DR} streaks (radial signatures of Z_{DR} that Z_{DR} alternate between rather high values and rather low values: Ryzhkov & Zrnić, 2007) related to the

depolarization effects of electrical canting ice particles (i Ventura et al., 2013; Hubbert et al., 2014; Schvartzman et al., 2022) were observed on the top of the thundercloud.

With the wide spread of dual-polarization weather radars, the signatures related to ice crystal orientation by the electric field have been well established. Based on the previous studies, the depolarization effects related to the electrical alignment of ice particles have been largely dominated by the propagation effects. Moreover, for the simultaneously transmitting and receiving horizontally and vertically polarized waves (SHV mode) scheme weather radar, which is the most widely used mode of dual-polarization weather radar, the measurements of Z_{DR}, ρ_{HV}, and the differential propagation phase shift (Φ_{DP}) are improved by eliminating inter-pulse variations and the Doppler effects (Scott et al., 2001). By using an X-band dual-polarization weather radar that transmitted circularly polarized waves and received simultaneously in horizontal and vertical polarization, Scott et al. (2001) showed that the electrical alignment directions of ice particles can be determined by changes in the polarization state between consecutive range bins caused by Φ_{DP} of vertically aligned ice particles. However, weather radar in SHV mode would introduce measurement biases due to the cross-coupling between the horizontal and vertical waves, especially in the measurement of Z_{DR} (Hubbert et al., 2010; Ryzhkov & Zrnić, 2007; Wang & Chandrasekar, 2006). Ryzhkov and Zrnić (2007) implied that the Z_{DR} signature depends both on the canting angle of particles and system differential phase shift on transmission and propagation differential phase shift, while the K_{DP} of aligned ice crystals is mainly dominated by the magnitude of the canting angle. Carey et al. (2009) explored the characteristics of K_{DP} and Z_{DR} related to ice particle orientation by modeling ice particles with the particle size distribution, mean canting angle, and different types of ice hydrometeor types. They concluded that electric fields and lightning potential are physically connected to the K_{DP} alignment signature. K_{DP} exhibits a linear relationship with particle concentration and a non-linear relationship with particle size. K_{DP} is a good indicator of electrical alignment signatures compared to Z_{DR}. Z_{DR} of vertical alignment ice particles could be masked by larger horizontal aggregates while K_{DP} is not. The K_{DP} seems to be a more robust parameter in SHV mode weather radar to study the signatures related to depolarization effects associated with the electrical alignment of ice particles.

Although dual-polarization radar can observe the depolarization effects of electrically aligned ice crystals in strong in-cloud electric fields, it is still difficult to observe the electrical alignment signatures in the whole electrification process of thunderstorms, and to observe the evolution of electric fields related to the upper charge region in the usual operational application. The first reason is due to the fast motion and rapid development of thunderstorms and the lightning discharges being intermittent and short duration. The observations by traditional polarimetric weather radars with mechanically scanned parabolic antenna are limited by volume scanning time. To study the depolarization effects related to the electrical alignment of ice crystals, weather radars need to point the antenna at fixed azimuth and either at a fixed elevation angle or within a small sector of elevation toward to suspected thunderstorm, then update the antenna position to track the electrically active cell. Most previous studies on electrical alignment signatures normally pointed the antenna in a fixed direction, or scanned on limited adjacent azimuth or elevation angles. The advantage of fixed location observation is that it can obtain sufficient dwell time to estimate polarized parameters and detect related signatures associated with each lightning activity. However, it is challenging to observe the electrical alignment signatures related to the upper charge region by traditional polarimetric weather radars within the evolution of thunderstorms in normal operation. On the other hand, the electrically active region of the thunderstorm was normally selected by taking the reflectivity of precipitation echoes for most previous researches, while the selected electrically active region was typically related to the main negative charge region. Or using other data as auxiliary indicators of an electrically active alignment region, such as the data of satellite communication links (Antar et al., 1980; Hendry & Antar, 1982), the lightning data (Metcalf, 1995) or data with another weather radar (Caylor & Chandrasekar, 1996). An observation from Krehbiel et al. (1984) showed a precise correlation between the first 15 negative IC lightning discharges of a localized storm and the updraft in the core of the storm, while a weaker radar echo extended up to and above the upper charge centers. This study implied that, during the early stages of electrification, the core of precipitation echo normally coincides with the center of the main negative charge region composited by graupel (Krehbiel, 1986; Krehbiel et al., 1984). It is worth noting that, in this study, a fast-scanning X-band vertical polarized radar using broad-band noise transmissions and a rapidly spinning antenna that can perform full volumetric hemispherical scans in 15–20 s was used to enable detailed observations of the rapid evolution processes in thunderstorms (Krehbiel & Brook, 1979). For well-developed thunderstorms, the discharge centers and paths are frequently (although not always) along the boundaries of high-reflectivity regions while tending to avoid the core

(Dye et al., 1986; Proctor, 1983). These probably indicate that during the evolution of thunderstorms, selecting a region only by the reflectivity-based method to study the electrical alignment signatures may not fully capture the features in changing electric fields related to the upper charge region.

Phased array weather radars have gained significant attention in meteorological applications with the advantage of high temporal and spatial resolution, especially in short-term severe convective weather system monitoring and early warning, such as tornadoes, microbursts, and thunderstorms (Adachi et al., 2016; Heinselman et al., 2015; Palmer et al., 2022; Ushio et al., 2015; Yoshida et al., 2017). Phased array weather radars will help better understand the evolution and electrification development of thunderstorms by providing more specific information on cloud microphysical evolution processes. In this paper, the dual-polarized multiparameter phased-array weather radar (MP-PAWR), located at Saitama University, is used to observe an isolated thunderstorm and analyze polarimetric parameters signatures associated with electrically aligned ice particles. The MP-PAWR is an X-band dual-linear polarized multiparameter phased array weather radar developed by Toshiba Corporation, Osaka University, and the National Institute of Communication and Technology (NICT). It can perform a volume scan of the whole sky in 30 s with a maximum detection range of 60 km, and a range resolution of 75m. The high spatial and temporal resolution of the MP-PAWR provides an effective way to observe the evolution and electrification life cycle of thunderstorms in normal operational applications. By introducing the composite K_{DP}, the electrical alignment signatures of ice particles before the first intracloud (IC) lightning flash are analyzed. The result allows us to explore the initial electrification process and vertical structure of the upper charge region in thunderstorms by the MP-PAWR. Section 2 is the introduction of data used in this paper and the methodology of data preprocessing and analysis. The observation and analysis results are presented in Section 3. A summary and discussions are shown in Section 4.

2. Data and Methodology

2.1. Lightning Data

Lightning data in this paper were obtained by the Lightning Detection Network (LIDEN) of the Japan Meteorological Agency (JMA). It consists of detection stations installed in 30 airports across the country receiving electromagnetic waves generated by lightning discharges, and of a central processing station that collects data from the detection station and determines the location of lightning discharges. The LIDEN system provides lightning data including types (intracloud or cloud-to-ground lightning), locations, and occurrence times of lightning discharges. We mainly employ IC flashes to focus on electrical alignment signatures of ice particles before the first IC lightning flash in the upper portion of the cloud.

2.2. Radar Data Processing

2.2.1. Dual-Polarized Multiparameter Phase Array Weather Radar

The MP-PAWR is a dual-linear polarized multiparameter phased array radar operated at X band with SHV mode, which provides parameters such as horizontal and vertical radar reflectivity (Z_H, Z_V), doppler velocity (V_H,V_V), doppler velocity spectrum width (W_H,W_V), and also polarization parameters such as differential reflectivity (Z_{DR}), differential propagation phase shift (Φ_{DP}), specific differential phase (K_{DP}), and correlation coefficient (ρ_{HV}). In a normal operational mode, the temporal resolution of a volume scan with 114 elevation angles is 30 s.

The MP-PAWR used in this paper is located at Saitama University in the metropolitan area of Japan (35.86158°N, 139.60908°E) at an altitude of 29.3 m above sea level. The capabilities and overall system description of the MP-PAWR were given by Takahashi et al. (2019) and Kikuchi et al. (2020). Also, comparison with a parabolic-type antenna X-band multi-parameter (X-MP) radar was performed by Asai et al. (2021).

2.2.2. Φ_{DP} Filtering and K_{DP} Estimation

To improve analysis accuracy, it is necessary to perform quality control of MP-PAWR polarization parameters first. In this paper, the quality control process is mainly applied to the differential propagation phase (Φ_{DP}), specific differential phase (K_{DP}), and horizontal reflectivity (Z_H).

There are many methods to filter Φ_{DP} from noisy total differential phase shift by removing backscatter differential phase shift (δ) and smoothing fluctuation of Φ_{DP}. Hubbert et al. (1993) proposed to use the method of Finite

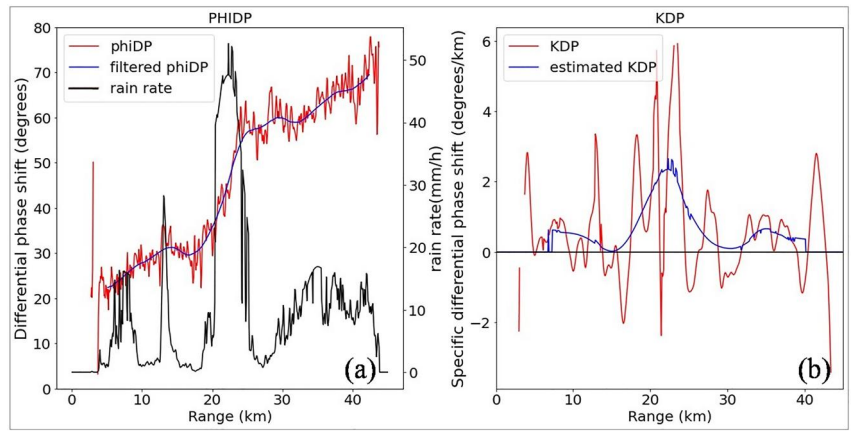

Figure 1. The radial profiles at an elevation angle of 4.99° and azimuth angle of 330° at 16:00:24 JST on 20 August 2019, Saitama University. (a) Radial profiles of raw Φ_{DP}, filtered Φ_{DP} and rainfall rate. The rainfall rate is estimated by the R (Z_H, K_{DP}) relationship from Suezawa et al. (2019), (b) radial profiles of raw K_{DP} and estimated K_{DP}.

Impulse Response (FIR) and Infinite Impulse Response (IIR) low-pass filter to process total differential phase shift, and Hubbert and Bringi (1995) proposed an iterative filtering technique based on this method, which can effectively eliminate backscatter differential phase shift (δ) existing in total differential phase shift. Giangrande et al. (2013) used the linear programming theory to eliminate the noise and ensure the processed total differential phase shift meets the condition of monotonically increasing with radial distance under the melting layer. K_{DP} could be estimated accurately from processed Φ_{DP}. Matrosov et al. (2006) used a linear regression method to derive K_{DP} from the slope of Φ_{DP}. In this paper, Φ_{DP} data provided by MP-PAWR are unwrapped already, we use the algorithm based on Hubbert and Bringi (1995) to filter Φ_{DP} and estimate K_{DP} by using the Colorado State University (CSU) RadarTools (Lang et al., 2007).

The algorithm of CSURadarTools to process raw Φ_{DP} calculate the standard deviation of Φ_{DP} at first, and only works when window length divided by gate spacing equals an even number (Lang et al., 2007). Considering that the depolarization effects of electrically aligned ice particles mainly depend on the differential propagation phase effects, the differential phase shift is accumulated along the radar radial. For weather radar with short wavelength, the backscatter differential phase δ is non-negligible for rain, whereas it can exceed 20° at X band for very large drops (Trömel et al., 2013). To better eliminate backscatter differential phase shift (δ) from the raw Φ_{DP} and obtain a reliable estimation of K_{DP} from smoothed Φ_{DP}, we employ an FIR range filter with a window length of 4.5 km and a standard deviation of differential phase $\sigma(\Phi_{DP})$ of 30°. This filtering process may result in the loss of the filtered Φ_{DP} in the several beginning and ending range bins along the radial paths. However, in the region near the radar, Φ_{DP} tends to be affected by the ground clutter, and Φ_{DP} in far-range bins tends to fluctuate erratically because of the low signal-to-noise ratio. The missed data will not affect the analysis from the observation of electrical alignment signatures. Finally, K_{DP} is estimated by the least squares method from the filtered Φ_{DP}, and calculated over a window whose length is inversely proportional to the Z_H values.

Figure 1 shows the radial profiles of rainfall rate, raw Φ_{DP}, raw K_{DP}, filtered Φ_{DP}, and estimated K_{DP}. The observation data was obtained by the MP-PAWR, at an azimuth angle of 330° and elevation angle of 4.99°, in a rain region below the melting layer at 16:00:24 JST on 20 August 2019. After quality-control processing, the filtered Φ_{DP} monotonically increases and the estimated K_{DP} keeps positive in the rain region below the melting layer. The estimated K_{DP} reaches a maximum of ~2.5°/km when the filtered Φ_{DP} grows rapidly between 20 and 30 km in a heavy rain region, while the peak rainfall rate reaches about 50 mm/hr. The altitude of the melting layer is about 5.5 km, based on sounding data at the Tateno site on 20 August 2019.

Figure 2 shows range-height-indicator (RHI) scan results of raw Φ_{DP}, filtered Φ_{DP}, raw K_{DP}, and estimated K_{DP} at an azimuth angle of 248.4° at 16:09:15 JST on 20 August 2019. The filtered Φ_{DP} and estimated K_{DP} are smoother and cleaner than the raw data. The discontinuity of raw Φ_{DP} and filtered Φ_{DP} at about 35° and 70° of elevation angle is mainly caused by different system differential phase shifts between different transmit beams of phased-array radar in electronically scanned elevations. It is obvious that Φ_{DP} decreased in the upper region of the cloud,

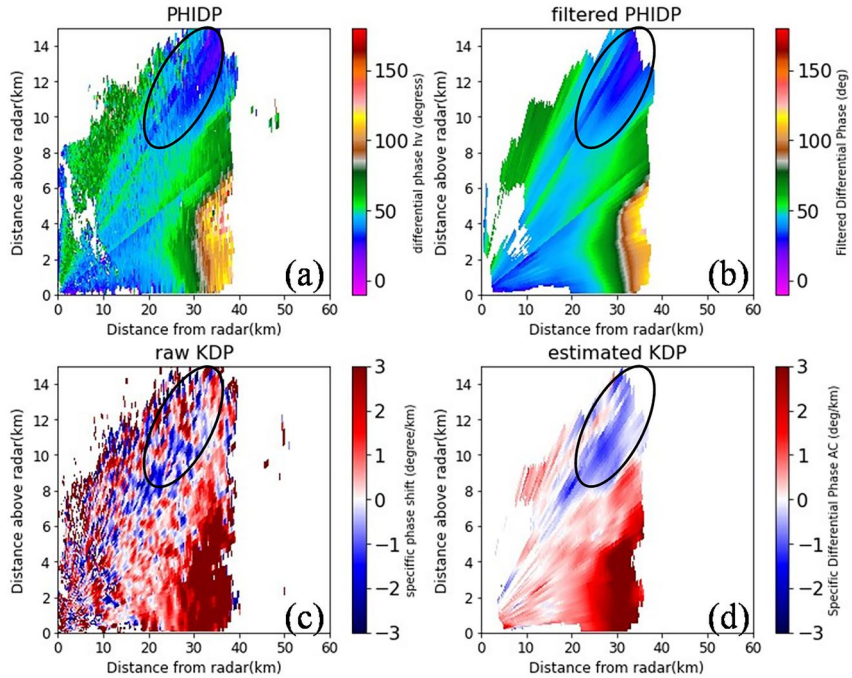

Figure 2. RHI scans of MP-PAWR at an azimuth angle of 248.4° at 16:09:15 JST on 20 August 2019, Saitama University. (a) Raw Φ_{DP}, (b) filtered Φ_{DP}, (c) raw K_{DP}, (d) estimated K_{DP}. The possible region with electrically aligned ice particles is marked as black ovals.

marked as black ovals in Figure 2, and K_{DP} in the same region are negative values as Figure 2d shows. The minimum K_{DP} at the 10 km height is less than −1°/km. Because small ice crystals tend to be more easily drifted up to the upper parts of the cloud top, and the K_{DP} of smaller, vertically aligned ice crystals will dominate over the K_{DP} of larger and horizontally aligned aggregates (Carey et al., 2009). These features should be attributed to the vertical alignment of ice crystals in strong electric fields.

Figure 3 shows constant-altitude plan-position indicator (CAPPI) images of horizontal reflectivity Z_H after attenuation correction and the estimated K_{DP} at an altitude of 10 km. The vertical cross-section results along the azimuth angle of 248.4° (black line in Figure 3) are shown in Figure 2. The IC lightning activities, as the black points marked, were detected in this region by the LIDEN system. The maximum Z_H is above 50 dBZ. The negative K_{DP} region in Figure 3b is associated with the lightning activities. The negative values of K_{DP} are largely due to the vertical alignment of ice crystals by electric fields. As Figures 2 and 3 show, the area of estimated K_{DP} is smaller than the area of raw K_{DP} and reflectivity, it is mainly caused by the process of filtering the raw Φ_{DP} as mentioned in above section. In the following part of this paper, if there is no special explanation, Φ_{DP} and K_{DP} are the filtered ones by the quality control process.

2.2.3. Attenuation Correction

X-band weather radars experience larger attenuation in rain than S/C-band radars, thus rain attenuation correction is needed, especially in convective rain events. The attenuation-correction procedures on MP-PAWR were introduced by using a method with K_{DP} (Asai et al., 2021), and the correction results showed that the MP-PAWR provides highly accurate precipitation observations developed in a short time, comparing with X-band multi-parameter (X-MP) radar in Japan. In this paper, the rain attenuation is corrected by using the ZPHI method (Bringi et al., 2001; Testud et al., 2000). The measured horizontal reflectivity Z'_H (mm^6/m^3) at a range r are related to corrected horizontal reflectivity Z_H (mm^6/m^3) as Equation 1, and the specific attenuation A_H (dB/km) is calculated according to Equation 2.

$$10\log_{10}\left[Z'_H(r)\right] = 10\log_{10}\left[Z_H(r)\right] - 2\int_0^r A_H(s)\,ds \quad (1)$$

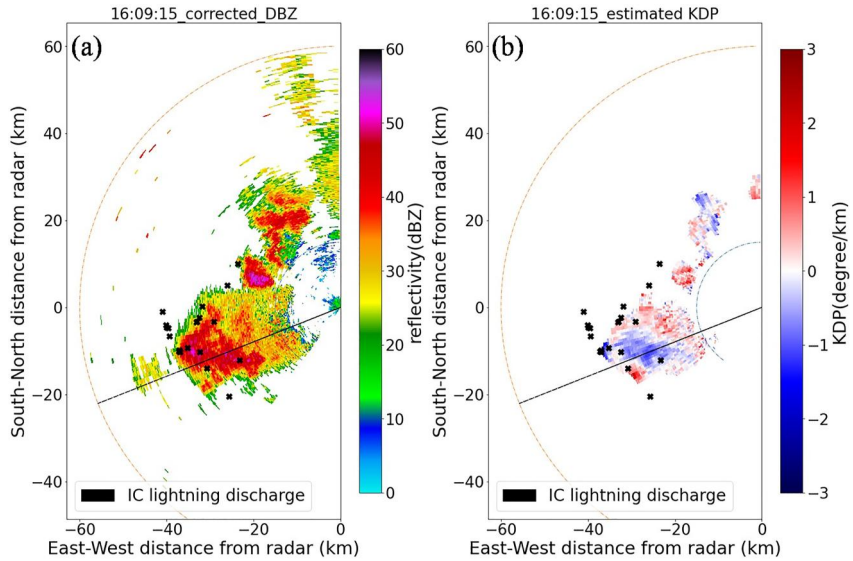

Figure 3. CAPPI images at an altitude of 10 km at 16:09:15 JST on 20 August 2019. (a) Corrected Z_H, (b) estimated K_{DP}. The black line is the azimuth angle of 248.4°. The blue and orange arcs represent 15 and 60 km away from MP-PAWR. The black point marks are the IC lightning discharge sources. The lightning discharge points fall out of the CAPPI results at altitude of 10 km is because the lightning discharge points were selected by the area of composite reflectivity at the −10°C layer (7 km), which the lightning discharge points distributed across all heights.

$$A_H(r) = \frac{\left[Z'_H(r)\right]^b \left(10^{0.1b\alpha\Delta\Phi_{DP}} - 1\right)}{I(r_1, r_0) + \left(10^{0.1b\alpha\Delta\Phi_{DP}} - 1\right) I(r, r_0)} \tag{2}$$

$$I(r_1, r_0) = 0.46b \int_{r_1}^{r_0} \left[Z'_H(r)\right]^b dr \tag{3}$$

$$I(r, r_0) = 0.46b \int_{r}^{r_0} \left[Z'_H(r)\right]^b dr \tag{4}$$

$\Delta\Phi_{DP} = \Phi_{DP}(r_0) - \Phi_{DP}(r_1)$, where r_1 and r_0 are represent the starting and ending range of a rain cell ($r_1 < r < r_0$). The coefficients α, and b of the A_H-Z_H relation are 0.254 and 1.143 respectively, which were used in attenuation correction with the X-MP radar (Park, Bringi, et al., 2005; Park, Maki, et al., 2005) and MP-PAWR (Asai et al., 2021).

Plan-position indicator (PPI) scan results of attenuation-corrected Z_H at 16:00:24 JST, 20 August 2019, are shown in Figure 4. The PPI scan was conducted at an elevation angle of 4.99°. Figure 5 shows the radial profiles of measured Z_H and attenuation-corrected Z_H at an azimuth angle of 330° (marked as the black line in Figure 4) and an elevation angle of 4.99°. The corrected Z_H closely matches the measured Z_H within a range of 20 km from the radar. Between the 20-km and 30-km range away from the radar, the difference between measured Z_H and corrected Z_H increases. At distances greater than 30 km, the corrected Z_H is more than 10 dB higher than the raw Z_H. It means that Z_H experiences significant attenuation between the 20-km and 30-km range, where the measured Z_H is larger than 40 dBZ. The trend of Z_H is consistent with the increasing Φ_{DP} in this region as Figure 1 shows, the overall reflectivity is recovered in the further region after the attenuation correction.

2.3. Analysis Method for Electrical Alignment Signatures of Ice Particles

Small ice particles tend to be more easily uplifted to the top parts of the cloud to form the upper positive charge region and vertically aligned by strong electric fields. Conversely, graupel, being typically larger and denser, is less likely to become vertically aligned. Moreover, the K_{DP} of larger horizontally oriented aggregates does not mask the K_{DP} of small vertically aligned ice crystals (Carey et al., 2009; Hubbert et al., 2014). These

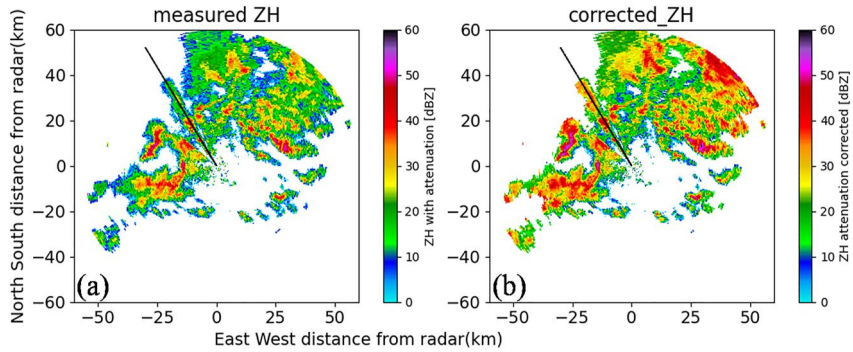

Figure 4. PPI scans of MP-PAWR at an elevation angle of 4.99° at 16:00:24JST on 20 August 2019. (a) Measured Z'_H (dBZ), (b) corrected Z_H (dBZ). The black line is the azimuth angle of 330°.

characteristics make the K_{DP} a good indicator of weather radar in SHV mode to observe the electrical alignment signatures of ice particles by strong electric fields in thunderstorms.

To explore the characteristics of the negative K_{DP} region associated with the upper charge region, including its distribution on azimuth and height, as well as the concentration of vertically aligned ice crystals, composite K_{DP} is introduced in this paper. It is defined as the minimum K_{DP} value in a vertical column of all elevation scans at each horizontal two-dimension grid point, similar to the definition of composite reflectivity (Witt et al., 1998). Considering that the main negative charge region distributes at approximately constant temperature levels between −10°C and −20°C (Dye et al., 1986, 1988; Krehbiel, 1986; Saunders, 1993; Saunders et al., 2006; Workman & Reynolds, 1949), we calculate the composite K_{DP} above the −10°C layer, representing the minimum K_{DP} in the vertical column at and above the −10°C layer, to investigate the features of upper positive charge region in early electrification stage.

Given that the negative K_{DP} values have a linear relationship with the concentration of vertically aligned ice particles by the strong electric field (Carey et al., 2009), it is evident that a higher concentration of electrically aligned ice particles corresponds to a stronger electric field. Moreover, the gross electric fields structure in thunderstorms undergoes slower changes compared to the changes in local electric field magnitudes causing lightning initiation. By calculating the average composite K_{DP} above different temperature layers, we can utilize the mean values of minimum K_{DP} within different regions in the upper parts of the isolated thunderstorm, specifically at and above different ambient temperature levels starting from the −10°C layer, to evaluate the vertical structure of electrically aligned ice particles with relatively high concentration during the electrification process in the thunderstorm. Consequently, a rough qualitative analysis of the vertical electrical structure of the dense upper charge region can be conducted based on these results. Additionally, as a comparative analysis, the average K_{DP} in a horizontal cross-section at different isothermal layers spanning from the −10°C layer to the cloud top could be calculated to analyze the vertical distribution of the upper charge region.

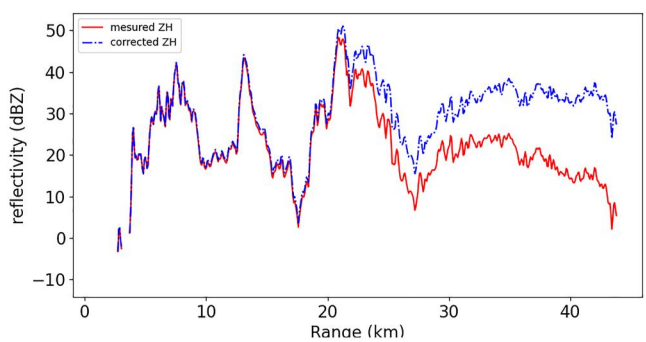

Figure 5. Radial profiles of measured Z_H (dBZ) (red line) and Z_H after attenuation correction (blue line) at an elevation angle of 4.99° and azimuth angle of 330° at 16:00:24 JST on 20 August 2019.

The reflectivity-based method is used to detect severe convection systems which could have the potential to produce lightning activities and thereby further be applied in lightning detection and warning by weather radars (Buechler & Goodman, 1990; Lund et al., 2009; Preston & Fuelberg, 2015; Woodard et al., 2011, 2012). The moderate reflectivity value (e.g., 30dBZ, 40dBZ) above the 0°C isothermal level is normally associated with the presence of graupel, which plays an important role in thunderstorm electrification. Buechler and Goodman (1990) used a criterion of 40 dBZ at −10°C to identify small thunderstorms and forecast the first lightning flash on 15 thunderstorm cases. Lund et al. (2009) concluded that the upper lightning initiation regions are near the 35 dBZ contours, with graupel distributing below and ice crystals above. Woodard et al. (2011, 2012) used different reflectivity thresholds, including 35 dBZ at −10°C, 40 dBZ at −15°C, and 45 dBZ at −20°C, to test a lightning initiation algorithm, and the threshold of reflectivity used the 40 dBZ at −15°C has the best performance. Preston and

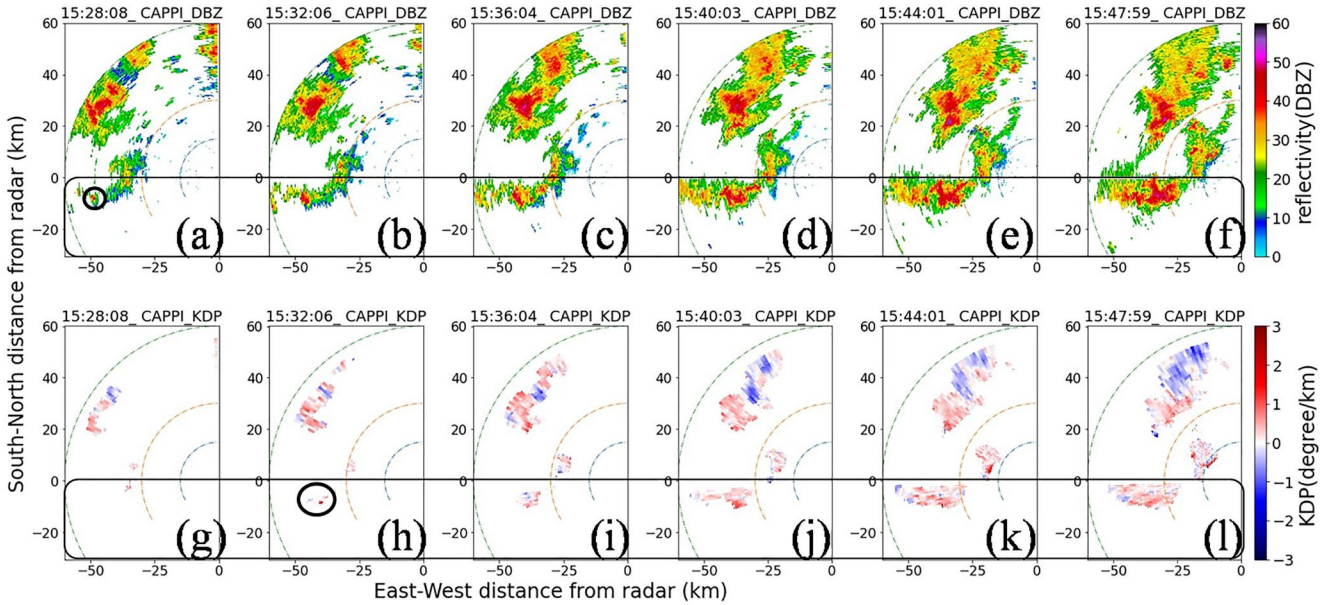

Figure 6. CAPPI results of Z_H and K_{DP} of the isolated thunderstorm at the −10°C layer on 20 August 2019, Saitama University. (a–f): Z_H, (g–l): K_{DP} from 15:28:08 to 15:47:59 JST. The time intervals are 4 min. Blue, orange, and green arcs represent 15 km, 30 km, and 60 km away from MP-PAWR. The early isolated thunderstorm echo at the −10°C layer is marked as black circles in (a, h). The analyzed isolated thunderstorm located in a region as a black box marked.

Fuelberg (2015) used the presence of graupel at different temperature levels (i.e., 0°C, −10°C and −20°C) in the mixed-phase region as a proxy for storm electrification, and showed that almost every flash initiation source was collocated with the presence of graupel at −10°C. They utilized the presence of graupel and horizontal reflectivity larger than 35 dBZ at the −10°C isothermal layer as threshold in lightning cessation algorithm.

In this study, a reflectivity criterion has been employed to identify the area with potential lightning activity. Considering that composite reflectivity can reveal important storm structure features and intensity trends of storms compared with base reflectivity, we use composite Z_H above the −10°C layer, where the reflectivity is larger than 40 dBZ at and above the −10°C isothermal layer, to define a two-dimension boundary of the analysis region in the isolated thunderstorm. Furthermore, to ensure data reliability, we screen out radar data with a correlation coefficient ρ_{HV} smaller than 0.8 in the selected region. By using composite K_{DP}, the electrical alignment signatures of ice particles in the upper parts of thunderstorms before the first IC lightning flash are analyzed. Based on sounding data at the Tateno site on 20 August 2019, the altitude of the −10°C, −20°C, −25°C and −30°C layers are about 7 km, 8.5 km, 9 km, and 10 km, respectively.

3. Observation and Analysis

3.1. Initial Electrification in the Early Developing Stage of an Isolated Thunderstorm

On 20 August 2019, there was a mesoscale convective system (MCS) moved from northwest to southeast of the MP-PAWR. To investigate the electrical alignment signatures of ice crystals before the first IC lightning flash, an isolated thunderstorm moving from the west of MP-PAWR was selected for analysis. The first IC flash occurred at 15:40:03 JST, at an azimuth angle of 263.2° and a distance of 42.6 km from the radar. CAPPI of Z_H and K_{DP} at the −10°C layer are shown in Figure 6.

Figure 6 illustrates the early developing stage of the isolated thunderstorm. After 15:28:08 JST, the analyzed isolated thunderstorm echo appeared at the −10°C layer with a maximum Z_H larger than 40 dBZ. Due to the Φ_{DP} filtering process mentioned before, the top height of K_{DP} at the same time remained below the −10°C layer. After 15:32:06, the isolated thunderstorm elevated and expanded its area at the −10°C layer, and the corresponding K_{DP} raised above the −10°C layer as shown by a black circle in Figure 6h. As time goes on, the area of the thunderstorm continued to increase. Considering that the purpose of this paper is to analyze the negative K_{DP}

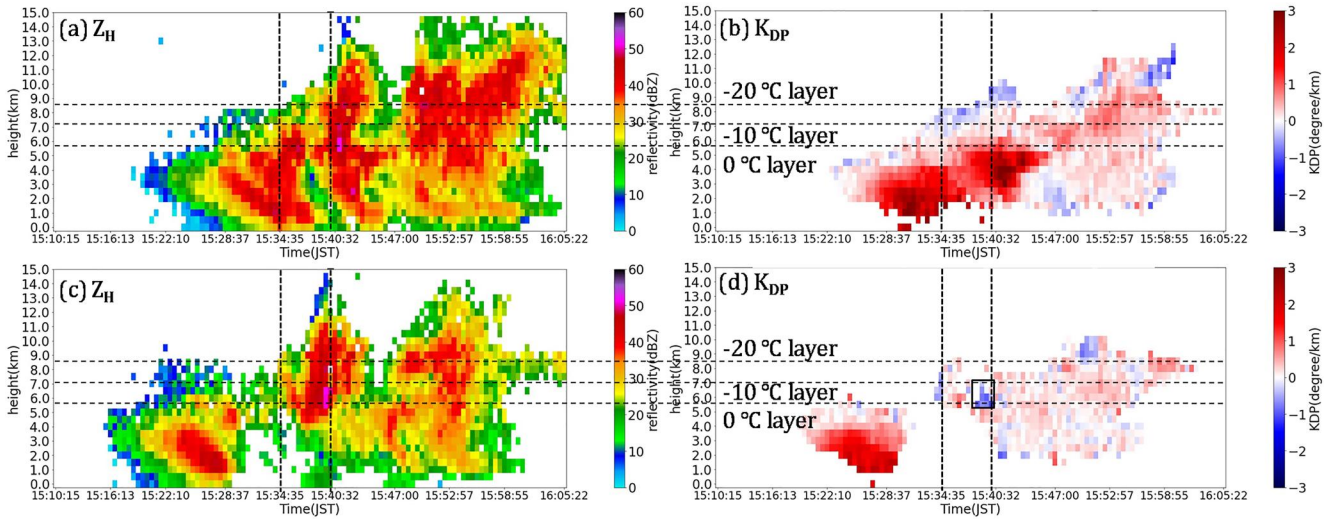

Figure 7. Time-height images of the isolated thunderstorm evolution from 15:10:15 to 16:05:22 JST. (a, b): Z_H and K_{DP} at a range of 40 km from the radar at a 260.4° azimuth, (c, d): Z_H and K_{DP} at a range of 42.6 km from the radar at a 262.8° azimuth. The time resolution is 30 s. The isothermal levels are marked as black dot lines horizontal in all panels. The left vertical black lines in all panels represent the time of 15:34:35 JST when the moderate reflectivity raised above the 0°C layer in (a), and the right vertical black lines in all panels mark the time of 15:40:03 JST which was the first IC lightning flash occurred. The black box in (d) marks a negative K_{DP} signature which appeared approximately 1.5 min before the first IC lightning flash between the 0°C layer and the −10°C layer.

signatures related to vertical alignment ice particles before the first IC lightning flash, K_{DP} results within the well-organized isolated thunderstorm after 15:32:06 are used to analyze.

Figure 7 shows the evolution of the developing stage of the isolated thunderstorm. The time resolution is 30 s, and the altitude resolution is 500 m due to computational limitations. After 15:59:25, the weakened and disappeared cloud echo was caused by the movement of the thunderstorm center toward to southeast.

Figures 7a and 7b exhibit the development of the isolated thunderstorm at a range of 40 km from the radar with a 260.4° azimuth, which is roughly along the azimuth with the most negative K_{DP} values at the layers ranging from the −10°C layer to the cloud top at 15:40:03 JST. As Figure 7a shows, it is evident that there was an updraft during the developing stage. The cloud grew upward and eventually reached a height of about 14.5 km. Especially after 15:34:35 JST (left black line in Figure 7a), the height of the echo with 40 dBZ reflectivity raised above the 0°C level and continued to move toward the −10°C layer, with continued elevated to exceed the −20°C layer when the first IC lightning flash occurred. It is obvious that negative K_{DP} appeared on the top of the cloud after 15:34:35 JST (left black line in Figure 7b) as shown in Figure 7b.

Figures 7c and 7d show the time evolution at a range of 42.6 km from the radar with a 262.8° azimuth, which represented the closest location to the occurrence of the first IC flash. There was a strong updraft with reflectivity larger than 40 dBZ above the 0°C layer. Moreover, 30 s before the first IC lightning flash, the maximum reflectivity exceeded 50 dBZ between the 0°C layer and the −10°C layer. From 15:38:32 JST to 15:40:03 JST, approximately 1.5 min before the first IC lightning flash, the K_{DP} values are negative between the 0°C layer and the −10°C layer, as shown by the black box in Figure 7d. Specifically, at 15:40:03 JST when the first IC flash occurred, the enhanced negative K_{DP} values that were less than −1°/km presented in the 0°C layer.

The vertical cross-sections of the isolated thunderstorm from 15:35:05 to 15:40:03 JST at a range of 42.6 km from the radar at azimuth from 240° to 270°are shown in Figure 8. It presents a detailed development in 6 min of the isolated thunderstorm near the location where the first IC lightning discharged before it occurred. Figures 8a–8f show the evolution of Z_H over a period of 6 min with a time interval of 1 min. The strong echo core grew upward and the altitude of 40 dBZ at the top of the echo core raised from about 7 to 11 km in 6 min, and the height of the cloud top raised from about 10 to 13 km in 6 min. Especially after 15:37:04 JST (Figure 8c), the region where reflectivity was larger than 40 dBZ extended above the −20°C layer and the area was getting wider. Figures 8g–8l show the evolution of K_{DP} at 1-min intervals. The positive K_{DP} core region where the maximum K_{DP} was larger than 4°/km corresponded with the strong echo core below the 0°C layer.

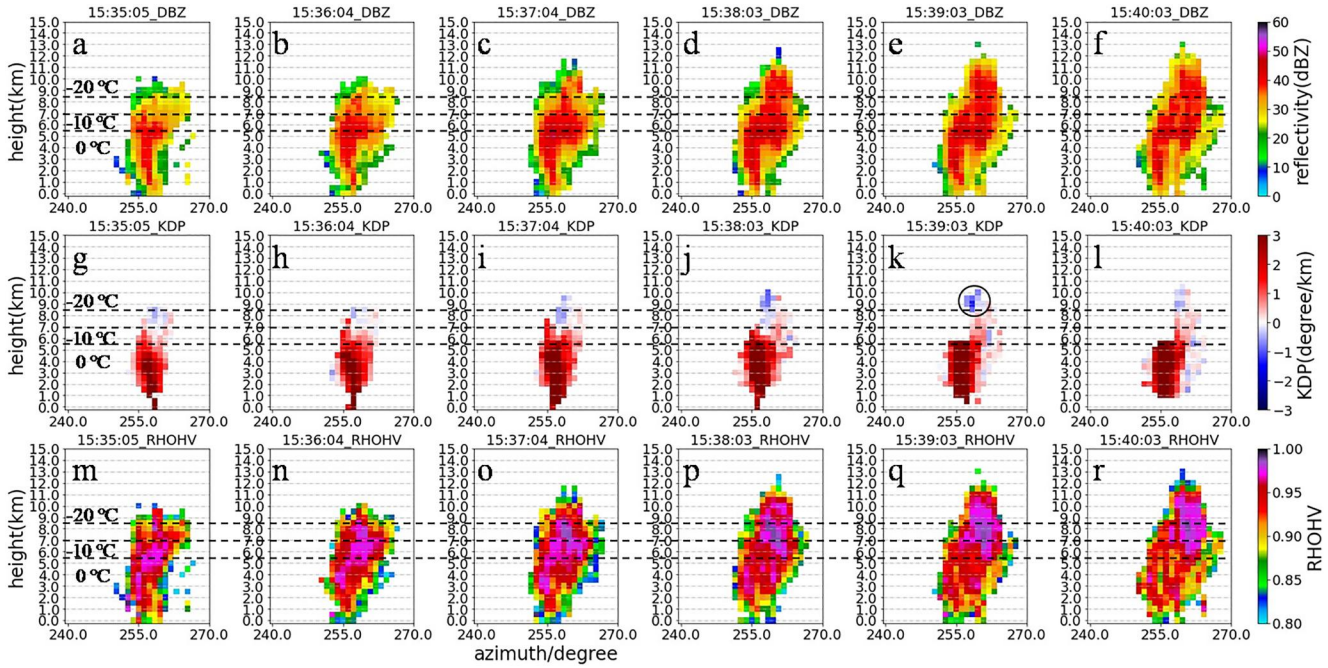

Figure 8. Vertical cross-sections at a range of 42.6 km from the radar at azimuth from 240° to 270° on 20 August 2019, Saitama University. (a–f): Z_H, (g–l): K_{DP}, (m–r): ρ_{HV} from 15:35:05 to15:40:03 JST. The time intervals are 1 min. The black circle in (k) marks a negative K_{DP} region with a minimum value of less than −1°/km.

Figures 8m–8r show the ρ_{HV} values which below the melt layer were around 0.925 while the ρ_{HV} values above the −10°C level were around 0.975. Under the melting layer, the positive K_{DP} region was associated with large reflectivity, and the ρ_{HV} values were around 0.925 means that the heavy rain probably was mixed with bigger drops or hailstones in this region. The positive K_{DP} region above the melt layer and below the negative K_{DP} region indicates that there were probably graupel, aggregates, and ice particles mixed. The positive values of K_{DP} may be largely related to the graupel because graupel is normally too large to be vertically aligned by strong electric fields and has the potential to mask ice crystal vertical alignment signatures in K_{DP} associated with strong electric fields (Carey et al., 2009). The negative K_{DP} region in the upper portions of the storm corresponded to the region where maximum reflectivity was about less than 40 dBZ and the ρ_{HV} values were larger than 0.95. This region maybe indicates the mixtures of aggregates and ice particles. Due to the K_{DP} of small vertically oriented ice particles dominate over larger horizontal alignment aggregates (Carey et al., 2009), the negative K_{DP} region was most likely related to the vertical orientation of ice particles due to strong electric fields. At 15:39:03 JST, 30 s before the first IC flash, marked as a black circle in Figure 8k, there is a region with negative K_{DP} less than −1°/km at 9 km height. It means more primarily vertically aligned ice particles in the enhanced electric fields on the cloud top.

Z_{DR} column has been used as an indicator of strong updraft and electrification. The Z_{DR} column is defined as a narrow vertical extension of positive Z_{DR} values above the 0°C isotherm level associated with the updrafts in deep moist convective storms (Kumjian et al., 2012, 2014). It is indicative of supercooled liquid drops lifted by the updraft. The Z_{DR} columns are likely sources of graupel embryos, which may form from the freezing of drops in these columns. The strong updrafts and the formation of graupel are favorable conditions for the electrification of thunderstorms and lightning flash initiation (Conway & Zrnić, 1993; Goodman et al., 1988; Kumjian et al., 2012, 2014; Lund et al., 2009; Woodard et al., 2011, 2012).

In the developing stage of the isolated thunderstorm, some Z_{DR} columns were observed. Taking one of them as an example which is marked as black ellipses in Figure 9, the reflectivity values (Z_H > 35 dBZ) associated with enhanced values of Z_{DR} (Z_{DR} > 3 dB), extended upward above the ambient 0°C layer. The signatures of the Z_{DR} column suggested the early electrification in the thunderstorm.

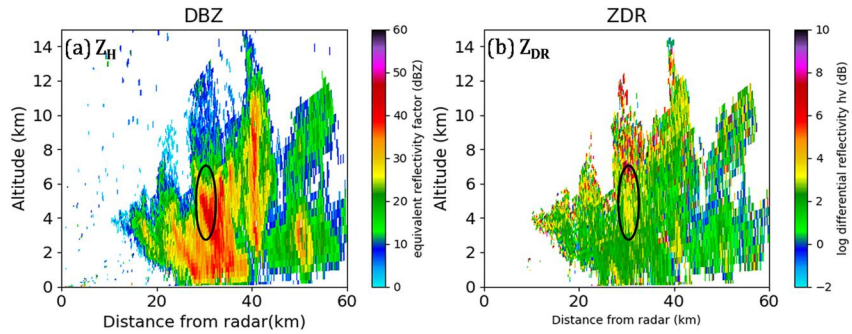

Figure 9. RHI scans of MP-PAWR along azimuth 260.4°, 15:40:03 JST on 20 August 2019. (a) Z_H, (b) Z_{DR}. The black ellipses in two panels show the observed Z_{DR} column.

3.2. Signature of Composite K_{DP} Before the First IC Lightning Flash

As Section 2 mentions, the composite K_{DP} above the −10°C layer is used to analyze the characteristics of negative K_{DP} associated with the vertical alignment signatures of ice particles before the first IC lightning flash in the upper parts of the isolated thunderstorm. Meanwhile, in the selected analysis region of the isolated thunderstorm, the mean values of composite K_{DP} are calculated above different isothermal layers ranging from −10°C to −30°C layer, which explore the concentration of vertically aligned ice particles in different upper volumes in the thunderstorm.

Figure 10 shows the horizontal cross-section results at the −10°C layer of composite Z_H, composite K_{DP}, and the CAPPI results of K_{DP} at the −10°C layer. The first IC flash occurred at 15:40:03 JST, indicated by the marked points in Figures 10e, 10k, and 10q, representing the azimuth locations of lightning discharges.

As Figures 10a–10f show, the Z_H of the isolated thunderstorm increases above the −10°C layer, with the maximum Z_H being larger than 50 dBZ after 15:34:05. Compared to the CAPPI results of K_{DP} shown in Figure 10g-l, the results of composite K_{DP} show a larger negative K_{DP} area and enhanced negative K_{DP} values at the −10°C layer as Figures 10m–10r show. It indicates that a great number of regions with higher concentrations of vertically aligned ice particles were distributed above the −10°C layer in the cloud. The larger negative K_{DP} region with more negative K_{DP} values, where the minimum K_{DP} was less than −1°/km as shown in Figure 10q, appeared near the location of the first IC lightning discharge. Conversely, no such obvious negative K_{DP} signatures are shown in Figure 10k. It implies that the use of composite K_{DP} provides a clearer representation of the negative K_{DP} signatures associated with the vertical alignment of ice particles in the upper parts of the cloud. Furthermore, it could indicate changes in azimuthal location and strength of the upper charge region in the thundercloud, which would facilitate observing the variations of electric field strength on vertical structures in thunderstorms.

As Figure 11a shows, the first IC lightning flash occurred at 15:40:03 JST (as marked by the right vertical black line). The mean composite Z_H which is larger than 40 dBZ reached and above the −10°C layer at 15:28:37 JST, then gradually increased to about 46 dBZ.

In Figure 11b, as mentioned before, the K_{DP} values after 15:33:06 (left black line in Figure 11b) are used for the analysis, and the composite K_{DP} values above the −40°C layer are not analyzed in this paper because that the top height of K_{DP} is below the −40°C layer before the first IC lightning flash. At 7 min before the first lightning flash, it is obvious that composite K_{DP} above the −10°C layer gradually decreased from approximately 0.3 to −0.2°/km in 3.5 min (from 15:33:06 to 15:36:34 JST), with the average composite K_{DP} above the −20°C layer decreasing, at 6 min before the first IC lightning flash, from about 0.5 to −0.65°/km in 5 min (from 15:34:05 to 15:39:03 JST). A similar signature also appeared above the −25°C layer, the average composite K_{DP} decreased from 0 to −0.4°/km between 15:35:05 to 15:35:36 JST, 5 min before the first IC lightning flash, followed with a decrease from about 0 to −0.7°/km in 1 min (from 15:37:34 to 15:38:33 JST) which is 2.5 min before first IC lightning flash. The average composite K_{DP} above the −30°C layer decreased at 2.5 min before the first IC lightning flash from about −0.4 to −0.8°/km in 30 s (from 15:37:34 to 15:38:03 JST) and continued to decrease from −0.65 to −1°/km in 1 min (from 15:38:33 to 15:39:33 JST). Notably, the composite K_{DP} above the −30°C layer reached the most negative value 30 s before the first IC lightning flash.

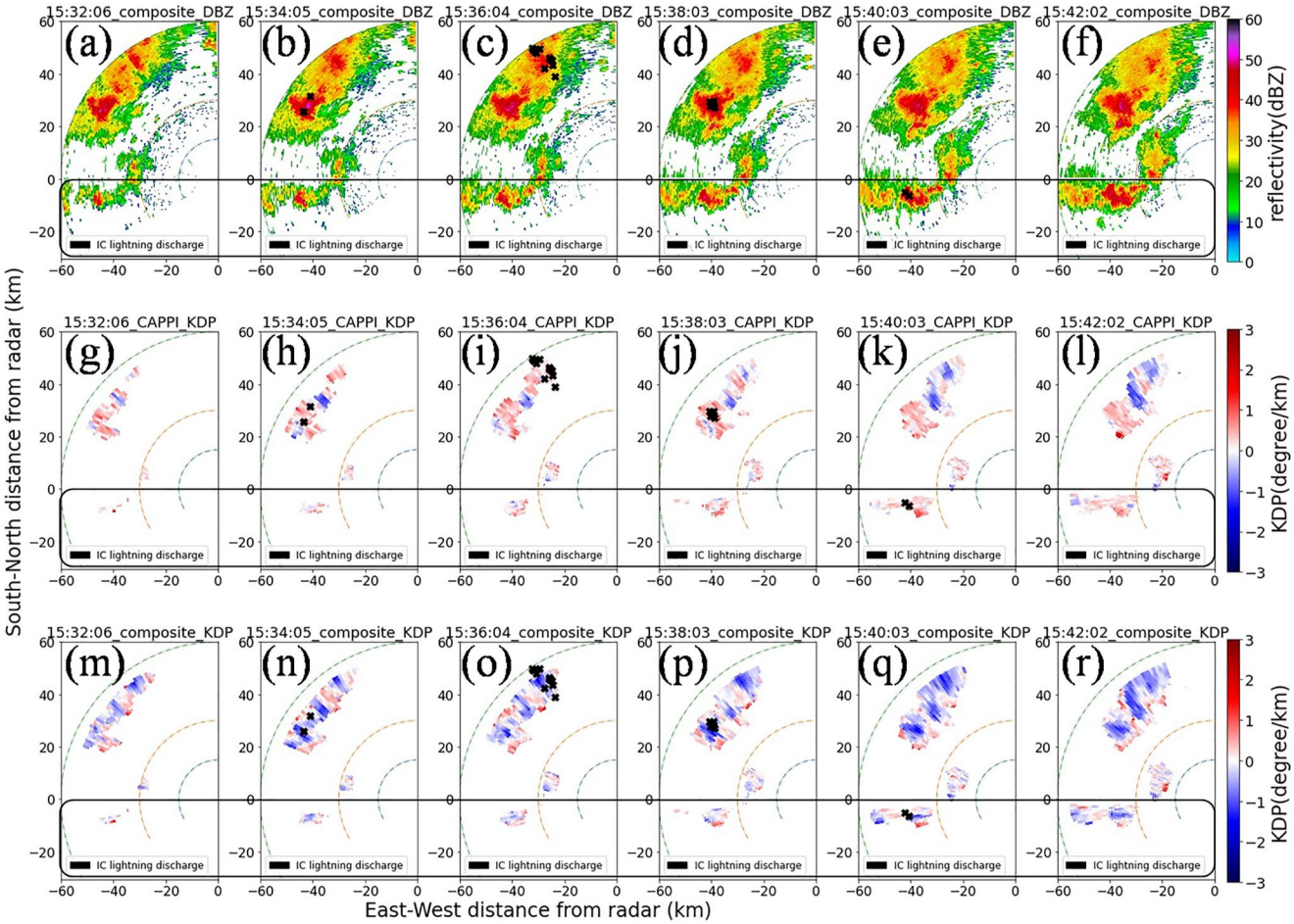

Figure 10. Horizontal cross-section images at the −10°C layer on 20 August 2019, Saitama University. (a–f): Composite Z_H, (g–l): CAPPI of K_{DP}, (m–r): Composite K_{DP}, from 15:32:06 to 15:42:02 JST, time intervals are 2 min. Three arcs represent 15, 30, and 60 km away from MP-PAWR. The black point marks are the IC lightning discharge sources. The analyzed isolated thunderstorm located in a region as a black box marked.

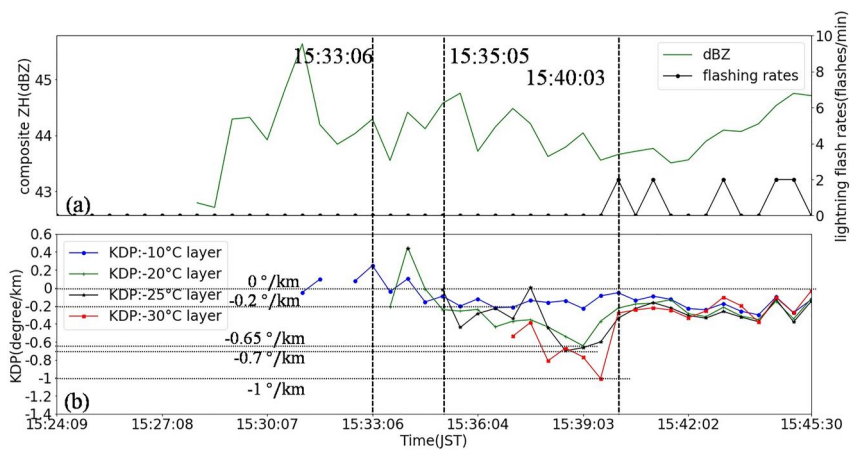

Figure 11. Average composite K_{DP} at and above different layers in the upper parts of the isolated thunderstorm. (a) Average composite Z_H values above the −10°C layer (the green line) and IC lightning flash rate (the black fold line), (b) average composite K_{DP} values above the −10°C to −30°C layer (The average composite K_{DP} at the −10°C layer: blue line, −20°C layer: green line, −25°C layer: black line, −30°C layer: red line).

The result shows that, before the first IC lightning flash, the mean values of composite K_{DP}, across different layers from the −10°C layer to the cloud top, gradually decreased, while the mean values of composite K_{DP} at a higher altitude were more negative than the values at a lower altitude. As the time approached the occurrence of the first IC lightning flash, the negative value of average composite K_{DP} appeared at higher altitudes and decreased to a more negative value compared to lower altitudes. For example, the average composite K_{DP} above the −10°C layer decreased from 0.3 to −0.2°/km 7 min before the first IC lightning flash, while the average composite K_{DP} above the −20°C layer decreased from 0.5 to −0.65°/km 6 min before the first IC lightning flash. Similarly, the average composite K_{DP} above the −25°C layer and the −30°C layer decreased from 0 to −0.7°/km 5 min before the first IC lightning flash, and from −0.4 to −1°/km 2.5 min before the first IC lightning flash, respectively.

These signatures probably indicate an evolution of the upper charge region associated with electrical-related ice particles in the initial electrification process during the early developing stage of a thunderstorm. The mean orientation of ice particles on the top of the cloud changed from horizontal to vertical alignment about 7 min before the first IC lightning flash. This change probably indicated a variation of the electric field, which was associated with the buildup of an upper charge region composed of charged ice particles. As the charged ice particles were carried upward by the updraft, the upper charge region raised from the −10°C layer, began approximately 7 min before the first IC lightning flash, and reached above the −30°C layer in 4.5 min. This accumulation at higher altitudes resulted in a gradual increase in the intensity of the electric field in the upper parts of the cloud that, in turn, would enhance the concentration of vertically aligned ice particles in the upper parts of the cloud. Correspondingly, the average composite K_{DP} exhibited a decrease before the first IC lightning flash.

The evolution of the upper charge region in the early electrification stage of the isolated thunderstorm could be qualitatively analyzed by the average composite K_{DP} at different isothermal layers. In this paper, the average composite K_{DP} above the −25°C layer began to decrease about 2 min after the decrease in average composite K_{DP} above the −10°C and the −20°C layers, which probably means the initial upper charge region built up under the −20°C layer (including the −20°C layer) and subsequently raised above the −25°C layer 2 min later. The average composite K_{DP} above the layers across the −10°C and the −30°C layers increased following with the first IC lightning discharge.

3.3. Signatures of Average K_{DP} Before the First IC Lightning Flash

Figure 12a displays a time-height analysis of the average K_{DP} values of the isolated thunderstorm, covering altitudes ranging from ground level to 15 km with a resolution of 500 m. The analysis region was selected using composite Z_H, where values exceeding 40 dBZ were observed above the −10°C layer. Notably, approximately 30 s before the first IC lightning flash, the average K_{DP} at the −30°C layer dropped below −1°/km, indicating an intensive concentration of vertically aligned ice particles accumulating in the top parts of the cloud resulting from stronger electric fields as the lightning event approached.

Figure 12b illustrates the evolution of the average K_{DP} at various altitudes. The occurrence of average K_{DP} at higher altitudes was delayed due to upward air motion. Before the first lightning flash at 15:40:03, the average K_{DP} values at and above the −20°C layers were predominantly negative, suggesting the presence of strong electric fields primarily at and above the −20°C layer.

Before the first IC lightning flash, average K_{DP} at altitudes between the −10°C and −30°C layer exhibited varying degrees of decrease. It noticed that the average K_{DP} values at the −10°C layer were almost positive, which is consistent with the conclusion from Mattos et al. (2016), who observed that storms with lightning showed strong positive K_{DP} in the layer from the 0°C and the −15°C layer. It is probably because graupel has the potential to mask negative K_{DP} signature related to vertically aligned ice particles by strong electric fields in the graupel-ice mixed region. The average K_{DP} at the −20°C layer was kept negative before the first IC lightning flash. It probably indicates that, during the early electrification stage, the upper charge region that was composed of ice particles accumulated around the −20°C layer, or/and uncharged ice crystals vertically aligned by the electric fields between the upper charge region and the main negative charge region. At the −25°C layer, the average K_{DP} decreased from 0.1°/km to −0.6°/km in 1 min (from 15:37:34 to 15:38:34), while at the −30°C layer, the average K_{DP} decreased from −0.4°/km to −1.0°/km 3 min (from 15:37:34 to 15:38:03) before the first lightning flash, further decreasing to −1.2°/km at 15:39:34 JST, 30 s before the first IC lightning flash. The average K_{DP} at the −20°C, −25°C, and −30°C layers increased with the first IC lightning discharge, indicating a weakening of the electric fields. These observations indicate that the average K_{DP} values became more negative at higher altitudes

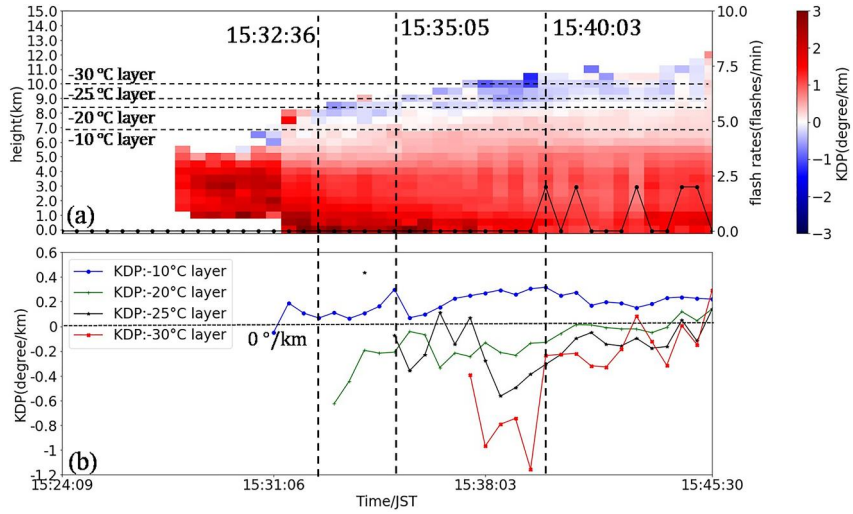

Figure 12. Time-height result of average K_{DP} of isolated thunderstorms. (a) Time-height image of average K_{DP}, the black fold line is IC lightning flash rate, and black horizontal lines mark the different isothermal levels; (b) average K_{DP} at different isothermal layers from the −10°C to −30°C layer (The K_{DP} at the −10°C layer: blue line, −20°C layer: green line, −25°C layer: black line, −30°C layer: red line), and the black horizontal dot line marks the reference line of K_{DP} equals 0°/km. After 15:32:36 JST (as the left vertical line marks), a negative K_{DP} region appeared at the top of the cloud and raised above the −25°C layer at 15:35:05 JST (as the middle vertical line marks). The right vertical line marks the first IC lightning flash that occurred at 15:40:03 JST.

as the first IC lightning flash approached, highlighting the enhanced negative K_{DP} signatures of vertically oriented ice particles associated with stronger electric fields, similar to the composite K_{DP} signatures observed before the first IC lightning flash.

4. Discussion and Conclusions

In this paper, an isolated thunderstorm is selected to analyze the electrical alignment signatures of ice particles in the upper parts of the thunderstorm before the first IC lightning flash. By introducing composite K_{DP}, the negative K_{DP} signatures associated with vertically oriented ice particles in strong electric fields are analyzed. The average composite K_{DP} across different layers, ranging from the −10°C to the −30°C isothermal layers, exhibited a descending trend from positive to negative values or from negative to more negative values before the first IC lightning flash. Subsequently, the average composite K_{DP} increased following the discharge of the first IC lightning. It is worth noting that, as the time approached the first IC lightning flash, the average composite K_{DP} demonstrated a further decrease to more negative values at higher altitudes. Specifically, the average composite K_{DP} started to decrease from a positive value to a negative value above the −10°C isothermal layer, approximately 7 min before the first IC lightning flash. The average composite K_{DP} above the −30°C isothermal layer reached the most negative value 30 s before the first IC lightning flash. Similar signatures are obtained by analyzing the average K_{DP} distributions in the upper parts of the thundercloud.

These results demonstrate that the mean canting angle of ice particles in the upper parts of the cloud changed from horizontal to vertical approximately 7 min before the first IC lightning flash. The concentration of vertically aligned ice particles progressively intensified with the strengthening electric field. The upper layers exhibited a higher concentration of electrically vertically oriented ice particles compared to the lower layers, probably due to the accumulation of more ice particles in the upper regions caused by updrafts. The concentration of electrically vertically oriented ice particles at the cloud top reached the maximum at about 30 s before the first IC lightning flash. This probably suggests that the electric field strength in the top parts of the cloud reached the maximum, potentially contributing to the initiation of the first IC lightning flash. With the occurrence of the first IC lightning flash, ice particles in the upper parts of the thunderstorm recovered to a horizontal or random alignment. Due to a short time from tens of milliseconds to a few seconds is taken to make the electrically aligned ice particles reorient after an abrupt change in electric fields caused by a discharge (Caylor & Chandrasekar, 1996; Hendry & McCormick, 1976; Zrnic & Ryzhkov, 1999) and the time resolution of MP-PAWR is 30 s, thus the signature that

the average composite K_{DP} increase following the first IC lightning flash indicates that the mean canting angle of ice particles restored from vertical to horizontal or more random orientation due to the weakening strength of the electric field after the lightning discharges.

Although uncharged ice particles can also be vertically aligned by the strong electric field, considering that the negative K_{DP} value exhibits a linear relationship with the concentration of vertical alignment of ice particles in the upper parts of the cloud, the increased concentration of vertically oriented ice particles indicates the presence of stronger electric fields resulting from a higher concentration of the upper charge region. Thus, the observed electrical alignment signatures of ice particles in the upper parts of the thunderstorm provide insights into the evolution of the upper charge region. Combined with the robust reflectivity signature of graupel in the mixed-phase region, the negative K_{DP} signatures which are physically connected to the electrical-related ice particles could be helpful to offer a description of the early electrification process of thunderstorms, which probably help to improve the probability of detecting the first IC lightning flash. The changes in the average composite K_{DP} values above different altitudes are related to variations in the height and concentration of the upper charge region, which is associated with the upper positive charge region in the typical bipolar charge structure of a thunderstorm. In this paper, 7 min before the first IC lightning flash, the upper charge region gradually formed under the −20°C layer (including the −20°C layer). With the upward motion of charged ice particles due to the updraft, the upper charge region subsequently accumulated above the −30°C layer in 4.5 min. It means the electric field built up and enhanced in the thunderstorms, resulting in an increased concentration of vertically aligned ice particles in the upper parts of the cloud. As analyzed in this paper, beneath the −20°C layer where ice particles are normally mixed with abundant graupel particles, the negative K_{DP} signatures of vertically aligned ice particles could be masked by the K_{DP} of graupel. At 7 min before the first IC lightning flash, the presence of a negative K_{DP} signature at the −20°C layer suggested that the electrification initiated below the −20°C layer (including the −20°C layer) at least 7 min before the first IC lightning flash.

In summary, due to the high spatial and temporal resolution, MP-PAWR in normal operation offers the capability to detect the rapid evolution of microphysical structures in thunderstorms and observe the specific electrification processes that are challenging for traditional mechanical weather radar to detect in normal operational volume scan mode. The introduction of the composite K_{DP} will help to observe the evolution of thunderstorm electrification processes more clearly, especially for confirming the onset of electrification combined with the presence of graupel in the mixed-phase region. The observation results in this paper illustrate the electrical alignment signatures of ice particles in the upper parts of the cloud before the first IC lightning flash, indicating an early electrification process where the electric fields build up and gradually intensify in the upper parts of the thunderstorm. However, there are still further studies that need to be done. The analysis of electrical alignment signatures of ice particles before the first IC lightning flash is based on a single isolated thunderstorm case in this study. In this case, the isolated thunderstorm was located approximately 30 km away from the radar before the first lightning flash, and the center of the thunderstorm is about 40 km away from the radar. The highest elevation angle was below 27° which allows the estimated K_{DP} can be used without correcting the K_{DP} bias with elevation angle. Nevertheless, the analysis of these signatures should be extended by correcting the elevation angle dependence bias of K_{DP} and validated using three-dimensional (3-D) lightning location data in more cases. Only in this way can the phased array weather radar fully utilize its ability to observe the lightning and thunderstorms in the entire sky.

Data Availability Statement

The Environmental sounding data are available on the website of the University of Wyoming. The LIDEN data and the MP-PAWR radar data on 20 August 2019, which was provided by NICT used in this paper are available in Wang (2023). The K_{DP} estimation algorithm is available in CSU_RadarTools version 1.3 (Timothy et al., 2019).

Acknowledgments
This study was supported by JSPS KAKENHI Grant 21H015920. The operation of the Saitama MP-PAWR was supported by Cross-ministerial Strategic Innovation Promotion Program (SIP) of the Cabinet Office. Data of the Saitama MP-PAWR is provided by National Institute of Information and Communications Technology (NICT).

References

Adachi, T., Kusunoki, K., Yoshida, S., Arai, K. I., & Ushio, T. (2016). High-speed volumetric observation of a wet microburst using X-band phased array weather radar in Japan. *Monthly Weather Review*, *144*(10), 3749–3765. https://doi.org/10.1175/MWR-D-16-0125.1

Antar, Y. M. M., Hendry, A., Schlesak, J. J., Olsen, R. L., & Berube, R. C. (1980). Ice-crystal depolarisation measurements at 28.6 GHz with simultaneous 16.5 GHz polarisation diversity radar observations. *Electronics Letters*, *16*(21), 808–809. https://doi.org/10.1049/el:19800575

Asai, K., Kikuchi, H., Ushio, T., & Hobara, Y. (2021). Validation of X-band multiparameter phased-array weather radar by comparing data from Doppler weather radar with a parabolic dish antenna. *Journal of Atmospheric and Oceanic Technology*, *38*(9), 1561–1570. https://doi.org/10.1175/JTECH-D-20-0213.1

Aufdermaur, A. N., & Johnson, D. A. (1972). Charge separation due to riming in an electric field. *Quarterly Journal of the Royal Meteorological Society*, *98*(416), 369–382. https://doi.org/10.1002/qj.49709841609

Bringi, V. N., Keenan, T. D., & Chandrasekar, V. (2001). Correcting C-band radar reflectivity and differential reflectivity data for rain attenuation: A self-consistent method with constraints. *IEEE Transactions on Geoscience and Remote Sensing*, *39*(9), 1906–1915. https://doi.org/10.1109/36.951081

Bringi, V. N., Knupp, K., Detwiler, A., Liu, L., Caylor, I. J., & Black, R. A. (1997). Evolution of a Florida thunderstorm during the convection and precipitation/electrification experiment: The case of 9 August 1991. *Monthly Weather Review*, *125*(9), 2131–2160. https://doi.org/10.1175/1520-0493(1997)125<2131:EOAFTD>2.0.CO;2

Brooks, I. M., & Saunders, C. P. R. (1994). An experimental investigation of the inductive mechanism of thunderstorm electrification. *Journal of Geophysical Research*, *99*(D5), 10627–10632. https://doi.org/10.1029/93JD01574

Buechler, D. E., & Goodman, S. J. (1990). Echo size and asymmetry: Impact on NEXRAD storm identification. *Journal of Applied Meteorology and Climatology*, *29*(9), 962–969. https://doi.org/10.1175/1520-0450(1990)029<0962:ESAAIO>2.0.CO;2

Carey, L. D., Petersen, W. A., & Deierling, W. (2009). Radar differential phase signatures of ice orientation for the prediction of lightning initiation and cessation. In *34th conference on radar meteorology M09-0584*.

Carey, L. D., & Rutledge, S. A. (2000). The relationship between precipitation and lightning in tropical island convection: A C-band polarimetric radar study. *Monthly Weather Review*, *128*(8), 2687–2710. https://doi.org/10.1175/1520-0493(2000)128<2687:trbpal>2.0.co;2

Caylor, I., & Chandrasekar, V. (1996). Time-varying ice crystal orientation in thunderstorms observed with multiparameter radar. *IEEE Transactions on Geoscience and Remote Sensing*, *34*(4), 847–858. https://doi.org/10.1109/36.508402

Conway, J. W., & Zrnić, D. S. (1993). A study of embryo production and hail growth using dual-Doppler and multiparameter radars. *Monthly Weather Review*, *121*(9), 2511–2528. https://doi.org/10.1175/1520-0493(1993)121<2511:ASOEPA>2.0.CO;2

Dye, J. E., Jones, J. J., Weinheimer, A. J., & Winn, W. P. (1988). Observations within two regions of charge during initial thunderstorm electrification. *Quarterly Journal of the Royal Meteorological Society*, *114*(483), 1271–1290. https://doi.org/10.1002/qj.49711448306

Dye, J. E., Jones, J. J., Winn, W. P., Cerni, T. A., Gardiner, B., Lamb, D., et al. (1986). Early electrification and precipitation development in a small, isolated Montana cumulonimbus. *Journal of Geophysical Research*, *91*(D1), 1231–1247. https://doi.org/10.1029/JD091iD01p01231

Dye, J. E., Winn, W. P., Jones, J. J., & Breed, D. W. (1989). The electrification of New Mexico thunderstorms: 1. Relationship between precipitation development and the onset of electrification. *Journal of Geophysical Research*, *94*(D6), 8643–8656. https://doi.org/10.1029/JD094iD06p08643

Giangrande, S. E., McGraw, R., & Lei, L. (2013). An application of linear programming to polarimetric radar differential phase processing. *Journal of Atmospheric and Oceanic Technology*, *30*(8), 1716–1729. https://doi.org/10.1175/JTECH-D-12-00147.1

Goodman, S. J., Buechler, D. E., Wright, P. D., & Rust, W. D. (1988). Lightning and precipitation history of a microburst-producing storm. *Geophysical Research Letters*, *15*(11), 1185–1188. https://doi.org/10.1029/gl015i011p01185

Gremillion, M. S., & Orville, R. E. (1999). Thunderstorm characteristics of cloud-to-ground lightning at the Kennedy Space Center, Florida: A study of lightning initiation signatures as indicated by the WSR-88D. *Weather and Forecasting*, *14*(5), 640–649. https://doi.org/10.1175/1520-0434(1999)014<0640:TCOCTG>2.0.CO;2

Heinselman, P., LaDue, D., Kingfield, D. M., & Hoffman, R. (2015). Tornado warning decisions using phased-array radar data. *Weather and Forecasting*, *30*(1), 57–78. https://doi.org/10.1175/WAF-D-14-00042.1

Hendry, A., & Antar, Y. M. M. (1982). Radar observations of polarization characteristics and lightning-induced realignment of atmospheric ice crystals. *Radio Science*, *17*(05), 1243–1250. https://doi.org/10.1029/RS017i005p01243

Hendry, A., & McCormick, G. C. (1976). Radar observations of the alignment of precipitation particles by electrostatic fields in thunderstorms. *Journal of Geophysical Research*, *81*(30), 5353–5357. https://doi.org/10.1029/JC081i030p05353

Hubbert, J., & Bringi, V. N. (1995). An iterative filtering technique for the analysis of copolar differential phase and dual-frequency radar measurements. *Journal of Atmospheric and Oceanic Technology*, *12*(3), 643–648. https://doi.org/10.1175/1520-0426(1995)012<0643:AIFTFT>2.0.CO;2

Hubbert, J., Chandrasekar, V., Bringi, V. N., & Meischner, P. (1993). Processing and interpretation of coherent dual-polarized radar measurements. *Journal of Atmospheric and Oceanic Technology*, *10*(2), 155–164. https://doi.org/10.1175/1520-0426(1993)010<0155:PAIOCD>2.0.CO;2

Hubbert, J. C., Ellis, S. M., Chang, W. Y., & Liou, Y. C. (2014). X-band polarimetric observations of cross coupling in the ice phase of convective storms in Taiwan. *Journal of Applied Meteorology and Climatology*, *53*(6), 1678–1695. https://doi.org/10.1175/JAMC-D-13-0360.1

Hubbert, J. C., Ellis, S. M., Dixon, M., & Meymaris, G. (2010). Modeling, error analysis, and evaluation of dual-polarization variables obtained from simultaneous horizontal and vertical polarization transmit radar. Part I: Modeling and antenna errors. *Journal of Atmospheric and Oceanic Technology*, *27*(10), 1583–1598. https://doi.org/10.1175/2010JTECHA1336.1

i Ventura, J. F., Honoré, F., & Tabary, P. (2013). X-band polarimetric weather radar observations of a hailstorm. *Journal of Atmospheric and Oceanic Technology*, *30*(9), 2143–2151. https://doi.org/10.1175/JTECH-D-12-00243.1

Kikuchi, H., Suezawa, T., Ushio, T., Takahashi, N., Hanado, H., Nakagawa, K., et al. (2020). Initial observations for precipitation cores with X-band dual polarized phased array weather radar. *IEEE Transactions on Geoscience and Remote Sensing*, *58*(5), 3657–3666. https://doi.org/10.1109/TGRS.2019.2959628

Krehbiel, P. R. (1986). The electrical structure of thunderstorms. In *The Earth's electrical environment* (pp. 90–113). Natl. Acad. Press.

Krehbiel, P. R., & Brook, M. (1979). A broad-band noise technique for fast-scanning radar observations of clouds and clutter targets. *IEEE Transactions on Geoscience Electronics*, *17*(4), 196–204. https://doi.org/10.1109/TGE.1979.294649

Krehbiel, P. R., Chen, T., McCrary, S., Rison, W., Gray, G., Blackman, T., & Brook, M. (1992). Dualpolarization radar signatures of the potential for lightning in electrified storms. In *9th international Conference of Atmospheric Electronic* (pp. 166–169).

Krehbiel, P. R., Chen, T., McCrary, S., Rison, W., Gray, G., & Brook, M. (1996). The use of dual channel circular-polarization radar observations for remotely sensing storm electrification. *Meteorology and Atmospheric Physics*, *59*(1–2), 65–82. https://doi.org/10.1007/BF01032001

Krehbiel, P. R., & Gray, G. (1993). Remote sensing of precipitation and electrification with a dual-polarization, coherent, wideband radar system (Final Report, 15 Jul. 1989–14 Jul. 1993).

Krehbiel, P. R., Rison, W., Thomas, R. J., Maggio, C., Marshall, T., Stolzenburg, M., et al. (2005). Lightning and dual-polarization radar structure of small convective storms. In *32nd conference on radar meteorology, Alvarado ABCD, American, hotel Albuquerque at old town, 15R.2*. Retrieved from https://ams.confex.com/ams/32Rad11Meso/webprogram/Paper96952.html

Krehbiel, P. R., Tennis, R., Brook, M., Holmes, E. W., & Comes, R. (1984). A comparative study of the initial sequence of lightning in a small Florida thunderstorm. In *Proceedings of the 7th international conference on atmospheric electricity* (pp. 279–285). American Meteorological Society.

Kumjian, M. R., Ganson, S. M., & Ryzhkov, A. V. (2012). Freezing of raindrops in deep convective updrafts: A microphysical and polarimetric model. *Journal of the Atmospheric Sciences*, *69*(12), 3471–3490. https://doi.org/10.1175/JAS-D-12-067.1

Kumjian, M. R., Khain, A. P., Benmoshe, N., Ilotoviz, E., Ryzhkov, A. V., & Phillips, V. T. (2014). The anatomy and physics of Z_{DR} columns: Investigating a polarimetric radar signature with a spectral bin microphysical model. *Journal of Applied Meteorology and Climatology*, *53*(7), 1820–1843. https://doi.org/10.1175/JAMC-D-13-0354.1

Lang, T. J., Ahijevych, D. A., Nesbitt, S. W., Carbone, R. E., Rutledge, S. A., & Cifelli, R. (2007). Radar-observed characteristics of precipitating systems during NAME 2004. *Journal of Climate*, *20*(9), 1713–1733. https://doi.org/10.1175/JCLI4082.1

Larsen, H. R., & Stansbury, E. J. (1974). Association of lightning flashes with precipitation cores extending to height 7 km. *Journal of Atmospheric and Terrestrial Physics*, *36*(9), 1547–1553. https://doi.org/10.1016/0021-9169(74)90232-3

Lund, N. R., MacGorman, D. R., Schuur, T. J., Biggerstaff, M. I., & Rust, W. D. (2009). Relationships between lightning location and polarimetric radar signatures in a small mesoscale convective system. *Monthly Weather Review*, *137*(12), 4151–4170. https://doi.org/10.1175/2009MWR2860.1

Matrosov, S. Y., Cifelli, R., Kennedy, P. C., Nesbitt, S. W., Rutledge, S. A., Bringi, V. N., & Martner, B. E. (2006). A comparative study of rainfall retrievals based on specific differential phase shifts at X-and S-band radar frequencies. *Journal of Atmospheric and Oceanic Technology*, *23*(7), 952–963. https://doi.org/10.1175/JTECH1887.1

Mattos, E. V., Machado, L. A., Williams, E. R., & Albrecht, R. I. (2016). Polarimetric radar characteristics of storms with and without lightning activity. *Journal of Geophysical Research: Atmospheres*, *121*(23), 14–201. https://doi.org/10.1002/2016JD025142

Mattos, E. V., Machado, L. A., Williams, E. R., Goodman, S. J., Blakeslee, R. J., & Bailey, J. C. (2017). Electrification life cycle of incipient thunderstorms. *Journal of Geophysical Research: Atmospheres*, *122*(8), 4670–4697. https://doi.org/10.1002/2016JD025772

McCormick, G. C., & Hendry, A. (1979). Radar measurement of precipitation-related depolarization in thunderstorms. *IEEE Transactions on Geoscience Electronics*, *17*(4), 142–150. https://doi.org/10.1109/TGE.1979.294641

Mendez, D. J. (1969). Optical polarization induced by electric fields of thunderstorms. *Journal of Geophysical Research*, *74*(28), 7032–7037. https://doi.org/10.1029/JC074i028p07032

Metcalf, J. I. (1992). *Radar observations of the effects of changing electric fields on the orientations of hydrometeors (No. 1100)*. Phillips Laboratory, Directorate of Geophysics.

Metcalf, J. I. (1993). Observation of the effects of changing electric fields on the orientation of hydrometeors in a thunderstorm. *Bulletin of the American Meteorological Society*, *74*(6), 1080–1083. https://doi.org/10.1175/1520-0477-74.6.1080

Metcalf, J. I. (1995). Radar observations of changing orientations of hydrometeors in thunderstorms. *Journal of Applied Meteorology and Climatology*, *34*(4), 757–772. https://doi.org/10.1175/1520-0450(1995)034<0757:ROOCOO>2.0.CO;2

Palmer, R., Bodine, D., Kollias, P., Schvartzman, D., Zrnić, D., Kirstetter, P., et al. (2022). A primer on phased array radar technology for the atmospheric sciences. *Bulletin of the American Meteorological Society*, *103*(10), E2391–E2416. https://doi.org/10.1175/BAMS-D-21-0172.1

Park, S. G., Bringi, V. N., Chandrasekar, V., Maki, M., & Iwanami, K. (2005). Correction of radar reflectivity and differential reflectivity for rain attenuation at X band. Part I: Theoretical and empirical basis. *Journal of Atmospheric and Oceanic Technology*, *22*(11), 1621–1632. https://doi.org/10.1175/JTECH1803.1

Park, S. G., Maki, M., Iwanami, K., Bringi, V. N., & Chandrasekar, V. (2005). Correction of radar reflectivity and differential reflectivity for rain attenuation at X band. Part II: Evaluation and application. *Journal of Atmospheric and Oceanic Technology*, *22*(11), 1633–1655. https://doi.org/10.1175/JTECH1804.1

Preston, A. D., & Fuelberg, H. E. (2015). Improving lightning cessation guidance using polarimetric radar data. *Weather and Forecasting*, *30*(2), 308–328. https://doi.org/10.1175/WAF-D-14-00031.1

Proctor, D. E. (1983). Lightning and precipitation in a small multicellular thunderstorm. *Journal of Geophysical Research*, *88*(C9), 5421–5440. https://doi.org/10.1029/JC088iC09p05421

Reynolds, S. E., Brook, M., & Gourley, M. F. (1957). Thunderstorm charge separation. *Journal of the Atmospheric Sciences*, *14*(5), 426–436. https://doi.org/10.1175/1520-0469(1957)014<0426:TCS>2.0.CO;2

Ryzhkov, A. V., & Zrnić, D. S. (2007). Depolarization in ice crystals and its effect on radar polarimetric measurements. *Journal of Atmospheric and Oceanic Technology*, *24*(7), 1256–1267. https://doi.org/10.1175/JTECH2034.1

Saunders, C. P. R. (1993). A review of thunderstorm electrification processes. *Journal of Applied Meteorology and Climatology*, *32*(4), 642–655. https://doi.org/10.1175/1520-0450(1993)032<0642:AROTEP>2.0.CO;2

Saunders, C. P. R. (2008). Charge separation mechanisms in clouds. *Planetary Atmospheric Electricity*, *137*(1–4), 335–353. https://doi.org/10.1007/s11214-008-9345-0

Saunders, C. P. R., Bax-Norman, H., Emersic, C., Avila, E. E., & Castellano, N. E. (2006). Laboratory studies of the effect of cloud conditions on graupel/crystal charge transfer in thunderstorm electrification. *Quarterly Journal of the Royal Meteorological Society: A journal of the atmospheric sciences, applied meteorology and physical oceanography*, *132*(621), 2653–2673. https://doi.org/10.1256/qj.05.218

Schvartzman, D., Bruning, E., Yu, T. Y., Chmielewski, V., Bodine, D., & Bluestein, H. B. (2022). Analysis of polarimetric spectral densities in severe thunderstorms for the identification of lightning-induced signatures.

Scott, R. D., Krehbiel, P. R., & Rison, W. (2001). The use of simultaneous horizontal and vertical transmissions for dual-polarization radar meteorological observations. *Journal of Atmospheric and Oceanic Technology*, *18*(4), 629–648. https://doi.org/10.1175/1520-0426(2001)018<0629:TUOSHA>2.0.CO;2

Suezawa, T., Kikuchi, H., Mega, T., Kim, D. K., Yoshikawa, E., Hayashi, S., & Ushio, T. (2019). An evaluation of rain attenuation correction for the multi parameter phased array weather radar. In *2019 AGU fall meeting, San Francisco, American, 2019*.

Takahashi, N., Ushio, T., Nakagawa, K., Mizutani, F., Iwanami, K., Yamaji, A., et al. (2019). Development of multi-parameter phased array weather radar (MP-PAWR) and early detection of torrential rainfall and tornado risk. *Journal of Disaster Research*, *14*(2), 235–247. https://doi.org/10.20965/jdr.2019.p0235

Takahashi, T. (1978). Riming electrification as a charge generation mechanism in thunderstorms. *Journal of the Atmospheric Sciences*, *35*(8), 1536–1548. https://doi.org/10.1175/1520-0469(1978)035<1536:REAACG>2.0.CO;2

Takahashi, T., & Miyawaki, K. (2002). Reexamination of riming electrification in a wind tunnel. *Journal of the Atmospheric Sciences*, *59*(5), 1018–1025. https://doi.org/10.1175/1520-0469(2002)059<1018:ROREIA>2.0.CO;2

Testud, J., Le Bouar, E., Obligis, E., & Ali-Mehenni, M. (2000). The rain profiling algorithm applied to polarimetric weather radar. *Journal of Atmospheric and Oceanic Technology*, *17*(3), 332–356. https://doi.org/10.1175/1520-0426(2000)017<0332:TRPAAT>2.0.CO;2

Timothy, L., Brenda, D., Nick, G., Cam, G., & Joseph, H. (2019). CSU-Radarmet/CSU_RadarTools: CSU_RadarTools v1.3 (version 1.3) [Software]. *Zenodo*. https://doi.org/10.5281/zenodo.2562063

Trömel, S., Kumjian, M. R., Ryzhkov, A. V., Simmer, C., & Diederich, M. (2013). Backscatter differential phase—Estimation and variability. *Journal of Applied Meteorology and Climatology*, *52*(11), 2529–2548. https://doi.org/10.1175/JAMC-D-13-0124.1

Ushio, T., Wu, T., & Yoshida, S. (2015). Review of recent progress in lightning and thunderstorm detection techniques in Asia. *Atmospheric Research*, *154*, 89–102. https://doi.org/10.1016/j.atmosres.2014.10.001

Vonnegut, B. (1965). Orientation of ice crystals in the electric field of a thunderstorm. *Weather*, *20*(10), 310–312. https://doi.org/10.1002/j.1477-8696.1965.tb02740.x

Wang, S. (2023). Electrical alignment signatures of ice particles before intracloud lightning activity detected by dual-polarized phased array weather radar (version 1) [Dataset]. *Zenodo*. https://doi.org/10.5281/zenodo.8409201

Wang, Y., & Chandrasekar, V. (2006). Polarization isolation requirements for linear dual-polarization weather radar in simultaneous transmission mode of operation. *IEEE Transactions on Geoscience and Remote Sensing*, *44*(8), 2019–2028. https://doi.org/10.1109/TGRS.2006.872138

Williams, E. R. (1989). The tripole structure of thunderstorms. *Journal of Geophysical Research*, *94*(D11), 13151–13167. https://doi.org/10.1029/jd094id11p13151

Williams, E. R., Weber, M. E., & Orville, R. E. (1989). The relationship between lightning type and convective state of thunderclouds. *Journal of Geophysical Research*, *94*(D11), 13213–13220. https://doi.org/10.1029/JD094iD11p13213

Witt, A., Eilts, M. D., Stumpf, G. J., Johnson, J. T., Mitchell, E. D. W., & Thomas, K. W. (1998). An enhanced hail detection algorithm for the WSR-88D. *Weather and Forecasting*, *13*(2), 286–303. https://doi.org/10.1175/1520-0434(1998)013<0286:AEHDAF>2.0.CO;2

Woodard, C. J., Carey, L. D., Petersen, W. A., & Roeder, W. P. (2011). 9.85 lightning initiation forecasting: An operational dual-polarimetric radar technique. Retrieved from https://ntrs.nasa.gov/citations/20120001475

Woodard, C. J., Carey, L. D., Petersen, W. A., & Roeder, W. P. (2012). Operational utility of dual-polarization variables in lightning initiation forecasting electron. *Journal of Operational Meteorology*, *13*, 79–102.

Workman, E. J., & Reynolds, S. E. (1949). Electrical activity as related to thunderstorm cell growth. *Bulletin of the American Meteorological Society*, *30*(4), 142–144. https://www.jstor.org/stable/26258148

Yoshida, S., Adachi, T., Kusunoki, K., Hayashi, S., Wu, T., Ushio, T., & Yoshikawa, E. (2017). Relationship between thunderstorm electrification and storm kinetics revealed by phased array weather radar. *Journal of Geophysical Research: Atmospheres*, *122*(7), 3821–3836. https://doi.org/10.1002/2016JD025947

Zrnic, D. S., & Ryzhkov, A. V. (1999). Polarimetry for weather surveillance radars. *Bulletin of the American Meteorological Society*, *80*(3), 389–406. https://doi.org/10.1175/1520-0477(1999)080<0389:PFWSR>2.0.CO;2